X-band airborne SAR tomography for forest volumes

Airborne X-band SAR Tomography for Forest Volumes

Fiona Muirhead[a], Iain H. Woodhouse[a], and Bernard Mulgrew[a]

[a]University of Edinburgh

ABSTRACT

We evaluate the usefulness of X-band, airborne (helicopter) data for tomography over forestry regions and discuss the use of compressive sensing algorithms to aid X-band airborne tomography. This work examines if there is any information that can be gained from forest volumes when analysing forestry sites using X-band data. To do so, different forest scenarios were simulated and a fast SAR simulator was used to model airborne multipass SAR data, at X-band, with parameters based on Leonardo's PicoSAR instrument. Model simulations considered varying factors that affect the height determination when using tomography. The main parameters that are considered here are: motion errors of the platform, the spacing of the flight paths, the resolution of the SAR images and plant life being present under the canopy (an understory). It was found that residual motion errors from the airborne platform cause the largest error in the tomographic profile.

Keywords: SAR, X-band, airborne, vegetation, tomography, sparsity

1. INTRODUCTION

SAR tomography, an extension of SAR Interferometry (InSAR), is an extremely useful technique that allows the user to obtain height information for multiple scatterers located within a single pixel in a stack of multipass SAR images. Literature surrounding airborne, X-band tomography is rare. Here we analyse the usefulness of X-band, airborne (helicopter) data for tomography over forestry regions. We simulate multiple images based on what would be acquired by Leonardo's PicoSAR, building on previous studies where real InSAR was carried out with helicopter data.[1] By using helicopter data we were able to analyse the outcome of tomography from a less stable platform. Here we discuss if compressive sensing can aid X-band airborne tomography. By combining short wavelength data, which is known to penetrate the canopy very little, with very high resolution imagery, we are able to determine if ground signals can be detected. Using compressive sensing algorithms we examine if is there any information that can be gained from forest volumes, or the ground beneath, when analysing forestry sites using X-band data. Forest heights are vital for improving vegetation mapping efforts, while the extraction of ground DEMs in vegetated areas with X-band would be revolutionary, therefore any information that can be gained from a new generation of compact SAR systems using new algorithms will aid in this effort.

Results from model simulations of varying factors that affect the heights determined through tomography are presented. The main parameters that are considered here are: the incidence angle of the system, motion errors of the platform, the spacing of the light paths, the resolution of the SAR images and plant life being present under the canopy (an understory).

Section 2 will discuss the forestry simulator, while the SAR simulator is outlined in Section 3. Section 4 details the need for persistent scatterers and Section 5 describes the compressive sensing methods used to carry out tomography. The results from applying tomography to the simulated SAR images of a forestry scenario are shown in Section 6.

Further author information: (Send correspondence to Fiona Muirhead)
E-mail: fiona.muirhead@ed.ac.uk, Telephone: 0131 343 5532

SAR Image Analysis, Modeling, and Techniques XVI, edited by Claudia Notarnicola, Simonetta Paloscia, Nazzareno Pierdicca, Edward Mitchard, Proc. of SPIE Vol. 10003, 1000308 · © 2016 SPIE
CCC code: 0277-786X/16/$18 · doi: 10.1117/12.2240645

2. FORESTRY SIMULATOR

To analyse the effects of different parameters on tomography over vegetated surfaces, a forestry simulator was developed. The forest simulator is based on the Polarimetric Radar Interferometry Simulator (PRIS).[2] The aim was to characterise the vertical distribution of radar reflectivity from a forest volume in a more representative way than a simple, uniform, homogeneous layer of random volume scattering. The three dimensional location and shape of the trees are important for realistic modelling[3,4] and this is included within PRIS. Individual tree architecture also has an impact on localised vertical reflectivity[5] but it is difficult to model with sufficiently high accuracy and requires specific information on tree architecture. Tree architecture is therefore not modelled here.

To characterise the tree size variation, a power law distribution was used to represent the variation of crown diameters for the number of trees in the scene (between the maximum and minimum crown diameters). A circle packing algorithm[6]was used to place the trees at random horizontal (x, y) positions in the scene using the diameters defined by the distribution, giving more smaller trees and fewer larger ones, as expected in a natural environment.

Three types of trees were modelled; ellipsoidal boreal, conical boreal and tropical. Crown volume is modelled as randomly distributed scatterers with homogeneous number density,[7] scattering and extinction properties. The rest of the 3D forest volume is modelled as either a gap, trunk (modelled as a cylinder of homogeneous scattering elements), or ground surface (which can be modelled as flat or sloped). Backscatter coefficients were chosen to given realistic normalised radar cross section across the forest canopy at X-band.[8] Trunks are modelled as cylinders, placed in the horizontal positions defined by the circle-packing function. All voxels (the representation of each discrete element of an array that a three-dimensional object is divided into) within the trunk are set to the trunk backscatter coefficient. The tree trunk double bounce in line of sight of the platform was modelled as the radar cross section from an ideal corner reflector.[9] The double bounce backscatter coefficient was placed on the ground plane in the voxel that is at the central edge of the trunk closest to the radar, and undergoes attenuation in both the incident and return paths. Once the forest voxels were generated they were rotated into the slant-range (antenna) coordinates by rotating the voxel array through the angle of incidence. The reflectivity was then determined in the rotated reference frame as this allows clear inclusion of attenuation (factored through range columns) since it allowed for the path length travelled through the forest canopy to be easily calculated. Once extinction was accounted for, the array is rotated back into azimuth, ground distance, height coordinates to be input into the radar simulator.

3. FAST SAR SIMULATOR

A fast SAR simulator was used to model multipass, X-band SAR data. Parameters were chosen to simulate real data from Leonardo's PicoSAR; a compact, lightweight, low cost, X-band airborne SAR system that can be placed on fixed wing aircrafts, helicopters and UAVs. In this study we analyse whether SAR tomography can be carried out from helicopter data, making the technique more accessible. Helicopter data suffers from the largest amount of motion error and therefore if the techniques works for helicopter data they should work for data collected from more stable platforms. The use of airborne platforms for environmental monitoring, as opposed to satellites, allows for rapid deployment to sites of interest. A high resolution (< 2m) airborne system could complement a global coverage satellite system by analysing results from a smaller localised area.[1]

The method for the fast SAR simulator is similar to a polar format algorithm in reverse. A 3D scene was specified containing information from the forest model (described in the previous section), including extinction. Starting with a rectangular grid from a 3D FFT of the scene, the data was interpolated to lie on a polar grid. Flight and waveform information, such as bandwidth and aperture length were chosen to define the polar grid. By defining multiple flight paths a stack of SAR images can be simulated. Platform motion that causes an unknown motion error that cannot be removed during motion compensation is added to the data. Decorrelation over the forestry canopy is also added. The fast SAR simulator is validated by comparing the impulse response of targets to those seen in real data.

4. PERSISTENT SCATTERERS

Since we are analysing the usefulness of X-band tomography over vegetation there will be a lot of noise (due to platform motion and scene decorrelation) in the stack of SAR images. Instead of carrying out tomography on each pixel we elected to analyse only the persistent scatterers (the most coherent and stable pixels over the image stack) as these pixels would give us the most accurate height profiles. Persistent scatterer interferometry is combined with tomography in[10] where a PS is considered to be a single point-like scatterer with high temporal coherence over the whole image stack. An inherent limitation associated with PSI in this sense is that since PS pixels are a single dominant scatterer within a resolution cell, pixels containing backscatter from multiple scatterers are rejected. This research looks at PSs from a different perspective. One reason for this is the use of higher resolution data, therefore there are less scatterers within a given resolution cell. Additionally the use of helicopters results in a less stable platform and means that there are fewer coherent pixels over the image stack. Thus PSs are vital to obtaining a tomographic solution. The novel method for selecting PS pixels by exploiting sparsity[11] does not reject pixels that contain more than one point scatterer in a resolution cell if the contribution is coherent and stable over the stack. This method is suitable for obtaining Dirac-delta functions for the heights of scatterers instead of a full tomographic profile.

5. COMPRESSIVE SENSING TOMOGRAPHY

SAR Tomography is applied to determine a height profile for coherent azimuth-range persistent scatterer pixels, i.e. pixels that are coherent and stable over the image stack. It is assumed that the number of scatterers in each pixel along the height domain is sparse and therefore compressive sensing routines can be utilised. The problem formulation is as follows:

$$\mathbf{f_s} = \mathbf{Ra} + \mathbf{n}, \tag{1}$$

Where $\mathbf{f_s}$ is the complex column vector for a given azimuth-range pixel on the m^{th} of M acquisitions, at aperture position b_m. $\mathbf{R}$ is composed of multiple steering vectors, $\mathbf{a}$ is the vertical distribution of scatterers in the elevation domain which we wish to determine and $\mathbf{n}$ is the noise term. The objective was to retrieve the height profile for each persistent scatterer pixel using an overcomplete representation and exploiting sparsity. The first algorithm for reconstructing the height profile in a given persistent scatterer pixel is a greedy algorithm. The least squares solution from such an algorithm is given by:

$$\hat{\mathbf{a}} = (\mathbf{R^H R})^{-1}\mathbf{R f_s}, \tag{2}$$

where $\hat{\mathbf{a}}$ is the height profile estimate. The estimation error $\hat{\mathbf{a_e}}$ is given by:

$$\hat{\mathbf{a_e}} = (\mathbf{R^H R})^{-1}\mathbf{R^H n}. \tag{3}$$

We seek a height distribution for the main scatterers within each pixel. The above method is the greedy forward regression technique; orthogonal least squares (OLS).[12] OLS has been shown to work well in noisy environments and has a convenient stopping criteria.[13] The parameter used in the stopping criteria, χ, is the critical value of the chi-squared distribution with one degree of freedom for a given level of confidence. $\chi = 8$ is chosen here. While the OLS method is computationally expensive, it can be applied to reconstruct height distributions as the data set at each pixel is relatively small.

The second algorithm that was used for comparison was an iterative hard thresholding (IHT) technique.[14] The height distribution is reconstructed by iterating over the following:

$$\mathbf{a^{[n+1]}} = \mathbf{H}(\mathbf{a^{[n]}} + \mu\mathbf{R}(\mathbf{f_s} - \mathbf{Ra^{[n]}})). \tag{4}$$

Where $\mathbf{H}$ is the hard thresholding operator that sets elements to zero if below a given threshold. μ is the step size, taken here to be $\mu = 0.3$. The number of iterations used for this research N was 25, however it was found that under most conditions $N = 15$ was sufficient.

6. RESULTS

To test the usefulness of X-band, airborne tomography over vegetation many different types of forests were produced and inserted into the SAR simulator with different input parameters (incidence angle, flight paths, number of passes). The stack of simulated SAR images were inserted into the tomography algorithm to calculate a height distribution for each persistent scatterer pixel. For this analysis a very basic forest was produced so that differences in the tomography solution could be easily identified. This technique allowed for one parameter to be altered at a time as to clearly compare the outcomes. The simple forest was made up of approximately 200 tree stands in one hectare, with all the trees having the same overall height (24m) and same canopy depth (2-4m), a typical simulated SAR image of this forest is shown in Figure 1. In this example there is no decorrelation or motion error added to the data. As the canopy was relatively thin extinction did not play a large role in the heights extracted from tomography. Typical extinction factors at X-band were obtained from previous studies.[8] Extinction has a greater effect when the canopy is thicker and is obscuring the ground. In this case the radiation has more to penetrate and hence less ground returns are detected.

A note on the terminology of persistent scatterers in the next sections: when no decorrelation or motion errors are added to the forest scene, parts of the vegetation can be considered persistent scatterers. Once decorrelation is accounted for then trunks, ground or corner reflectors on the surface are more likely to be persistent as these objects are more stable over time. In the following simulations 2000 persistent scatterers are detected in each stack of multipass SAR images; this is approximately 1% of the total number of pixels in each image.

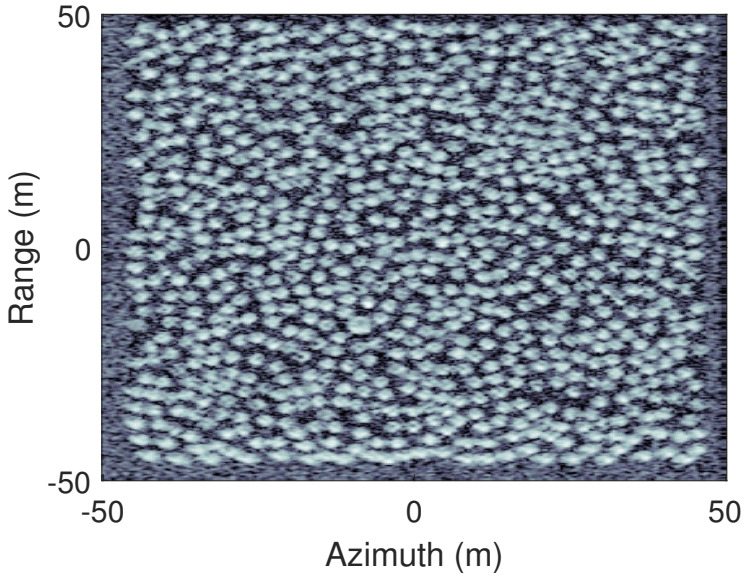

Figure 1. One of the multipass simulated SAR images of the basic forest volume.

6.1 Flight Paths

The fast SAR simulator uses typical parameters from PicoSAR. An incidence angle of 15° was used which is slightly larger than that used by PicoSAR but is still very much less than typical angles used from satellite systems. This highlights one of the main differences between the airborne and satellite platforms. The flight paths considered had to allow for suitable resolutions and ambiguities from the tomography solution. The Rayleigh resolution is given by:

$$\rho_a = \frac{\lambda r}{2B}, \tag{5}$$

where $B = b_{max} - b_{min}$. The ambiguity of the height profile that can be determined is given by:

$$\Delta A = \frac{\lambda r}{2\delta b}, \tag{6}$$

where δb is the closest spacing between apertures. For this simulation a typical platform height of 1700m and a range of 6000m with 90 passes spaced at 2m apart will provide a spatial resolution of 0.5m in the height domain and an ambiguity of 50m. This perfect scenario allows for a perfect retrieval of the tomographic profile. From this profile you get equal amounts of canopy and ground detected, see Figures 2 and 3. The canopy is detected at 20m and the ground at 0m. The canopy is detected at 20m instead of 24m due to the canopy being modelled as ellipsoidal and due to there being a small amount of penetration through the canopy at X-band. Reducing the flight paths from 2m apart to 4m increases the amount of ground detected.

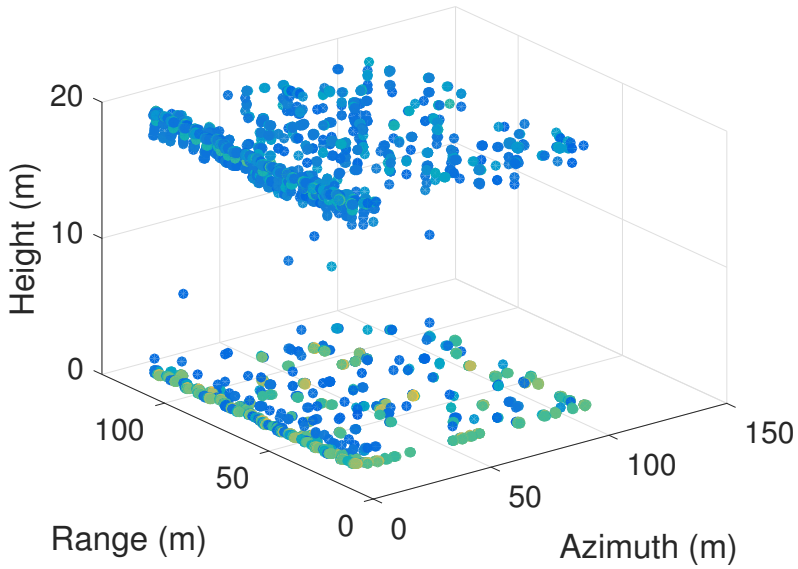

Figure 2. The tomographic retrieval from the simple forest scenario with 90 passes at 2m baselines. No motion error or decorrelation is added to this best case scenario.

It is clear that 90 passes is unrealistic for such a system, therefore to achieve the required resolution and ambiguity coprime sampling is utilised. Coprime sampling reduces the number of passes to 10. Using coprime sampling we get more false detections (scatterers placed between 1m and 18m) however the overall height of canopy and ground is still very clear, see Figure 4. This figure highlights the first scatterer detected in each PS pixel. The motion error noise mainly affects the heights detected for the smaller scatterers within each PS pixel.

Reducing the total span of the flight paths decreases the resolution. It was found that decreasing the span to 40m gave a resolution of 2.4m and was not suitable for finding an accurate tomographic profile. A baseline span of 80m results in a resolution of 1.2m. This set up results in mainly detecting ground and again is not suitable. A large enough span is needed to get fine enough resolution but also have enough passes so that the ambiguity on the ground is great enough to detect the height of the forest.

6.2 Image Resolutions

By increasing the image resolution it may be possible to see below the canopy even at short wavelengths such as X-band. Having fine resolution, for example 0.5m resolution, allows for extra ground to be picked up between trees. SAR images are simulated at 0.2m range resolution and 0.5m azimuth resolution for the basic forest scene. These resolutions allows the gaps within the forest canopy to be visible and for ground returns to be detected. With such a basic scene making the image resolution coarser than this means that many pixels contain returns from the ground and canopy. In this case it is mainly pixels around the edge of the scene that just contain ground signal that are detected as persistent scatterers, as seen in Figures 5 and 6.

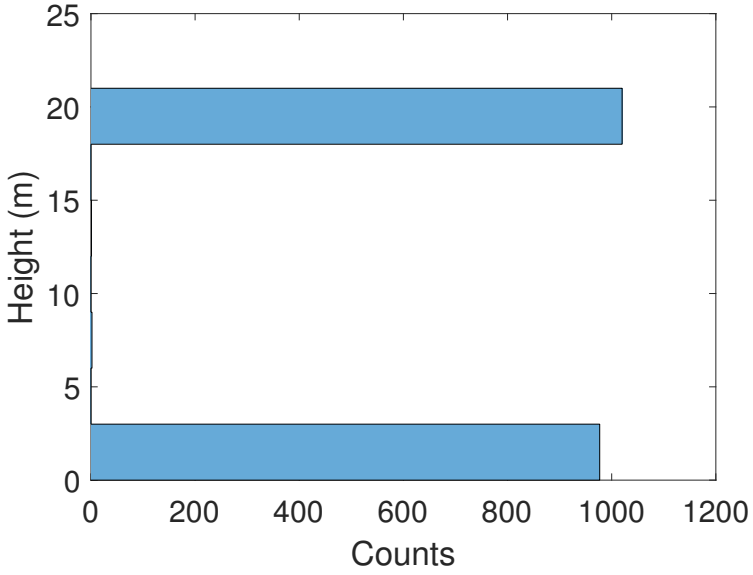

Figure 3. A histogram of the heights retrieved from the simple forest scenario with 90 passes at 2m baselines. No motion error or decorrelation is added to this best case scenario.

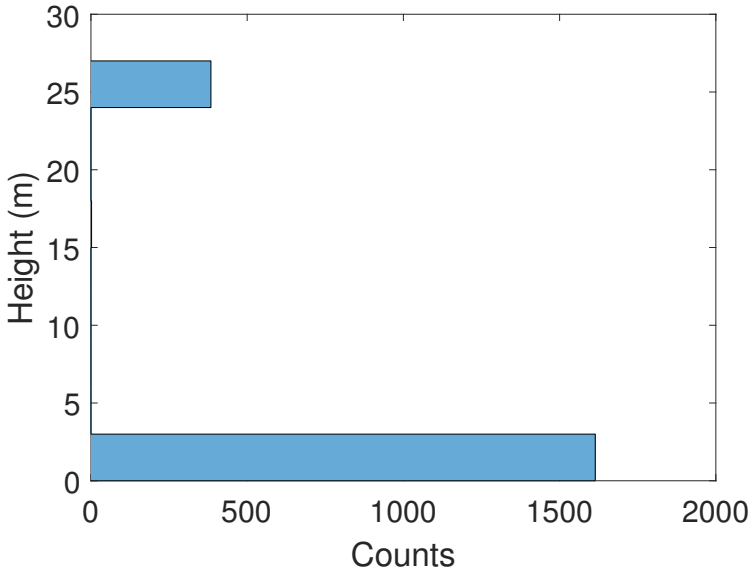

Figure 4. A histogram of the heights retrieved from the simple forest scenario with coprime baselines. No motion error or decorrelation is added to this scenario.

6.3 Decorrelation

This section analyses whether a bright, coherent object, such as a corner reflector, could be detected in the presence of decorrelation. In the simulation all types of decorrelation are accounted for using one decorrelation term. Decorrelation is more extensive in the canopy than on the ground and so a larger amplitude and phase change is added to the canopy to simulate decorrelation. Decorrelation on the scale of a wavelength has the potential to greatly degrade the quality of the tomographic profile. Adding in a small amount of decorrelation to the canopy makes no difference to the overall tomographic profile. Adding in a large amount of decorrelation

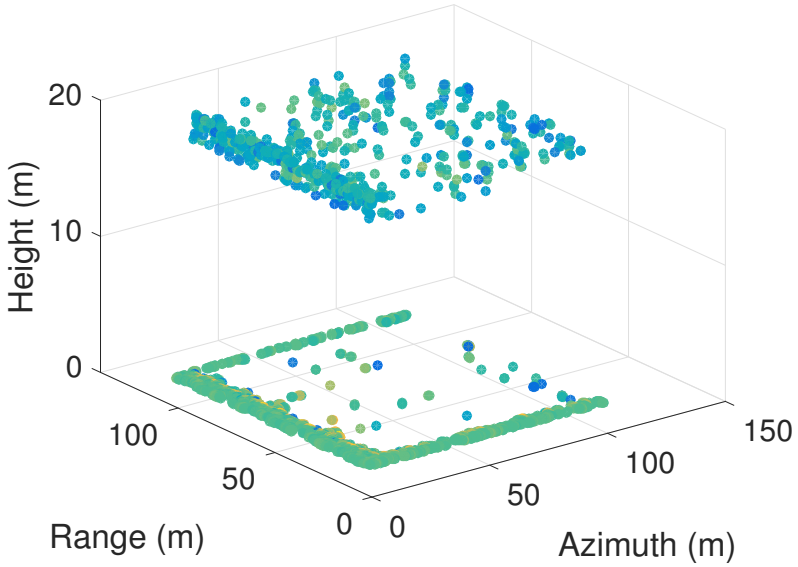

Figure 5. The tomographic retrieval from the simple forest scenario with coarser resolution. No motion error or decorrelation is added to this scenario.

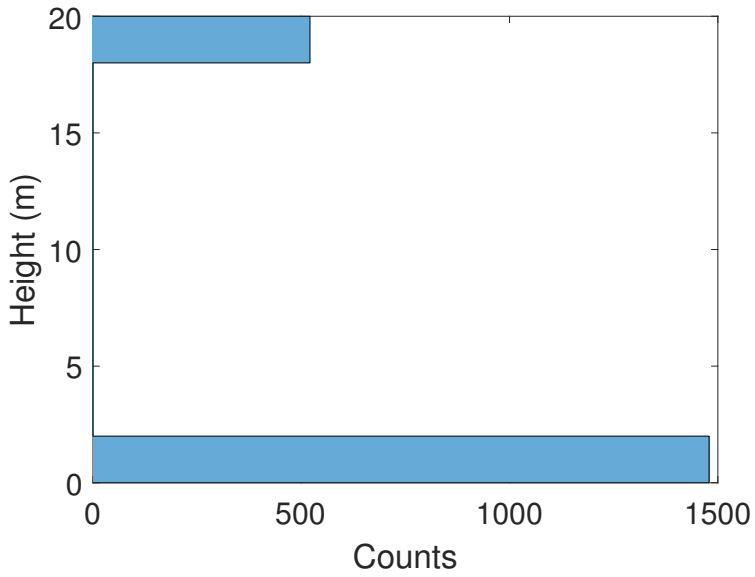

Figure 6. The histogram of height retrieved from the simple forest scenario with coarser resolution. No motion error or decorrelation is added to this scenario.

results in many false detections, see Figure 7 however canopy and ground scatterers are still clear in the first scatterer detected in each pixel, as seen in Figure 8. Doubling the ground reflectivity approximately doubles the number of ground returns detected in the tomographic profile, even with a large amount of decorrelation. Overall decorrelation increases the number of false heights detected but by just analysing the largest scatterer present in each persistent scatterer pixels allows for an approximation of ground and canopy position.

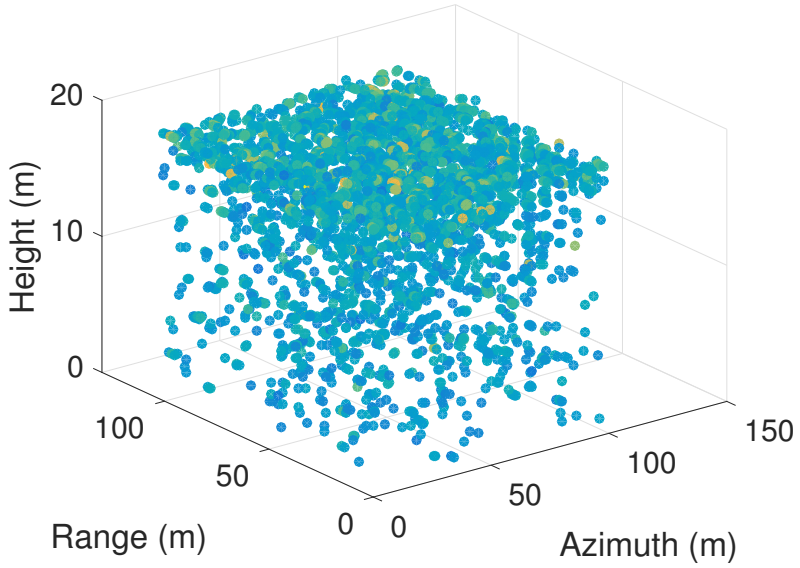

Figure 7. The tomographic retrieval from the simple forest scenario with a large amount of decorrelation added to the canopy.

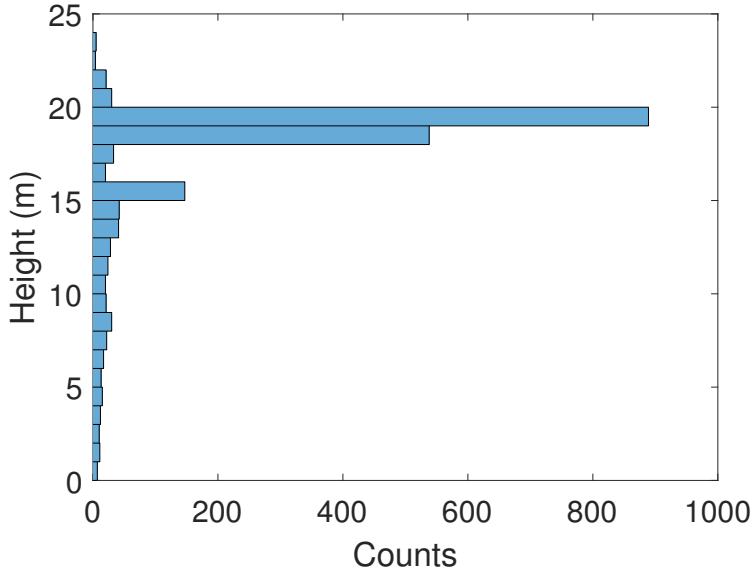

Figure 8. The histogram of heights retrieved from the simple forest scenario with a large amount of decorrelation added to the canopy.

6.4 Motion Errors

The amount of time for each pulse to travel from the SAR system to the patch centre and back needs to be known for each transmission point along the synthetic aperture.[15] For satisfactory SAR images the relative uncertainties in the distance R_0 has to be a fraction of a wavelength of the SAR centre frequency. Navigational systems are used to estimate R_0 for each pulse using IMUs as these have high enough frequency to gain information for each pulse. Navigational systems also utilise GPS to increase the accuracy, however the frequency for GPS is much lower. Higher azimuth resolution images require longer synthetic apertures. These longer apertures give the

IMU more time to drift during collection. To overcome such errors autofocus algorithms are employed, however residual motion errors are still present within stacks of SAR images for tomography. Compact SAR systems are limited in the IMU that they can use as it has to be low mass and small size to fit on the system.

In real data the platform does not fly a perfect linear path, especially using a helicopter platform, therefore motion errors have to be added to the simulation. Large scale motion errors are accounted for using motion compensation yet there are still residual motion errors that have to be included. These errors can be accounted for by autofocus however this is not a perfect solution. Any residual motion (which is different between passes) will cause errors for the tomography output since the steering vectors will not be accurately known. This section discusses what level of motion errors are acceptable to still get an accurate tomographic result. Navigational errors are cumulative therefore the motion error is taken to be the cumulative sum of a zero-mean, normally distributed random variable.[16] A smoothing filter is applied over the sum of a few hundred milliseconds. Previous modelling takes the standard deviation of the random errors to be 5cm per pulse.[16]

It should be noted that the highest amount of motion errors occur during windy weather. Wind also causes decorrelation in vegetation, therefore such weather has a twofold effect. As we are simulating typical scenarios from helicopter data the motion errors are higher than in other SAR datasets. Initially we add a small error to each x, y, z platform position on each pulse. The final error in range on each pulse is shown in Figure 9. This results in some false detections at 15m in the tomographic profile however still gives a clear indication of canopy and ground position, as shown in Figure 10.

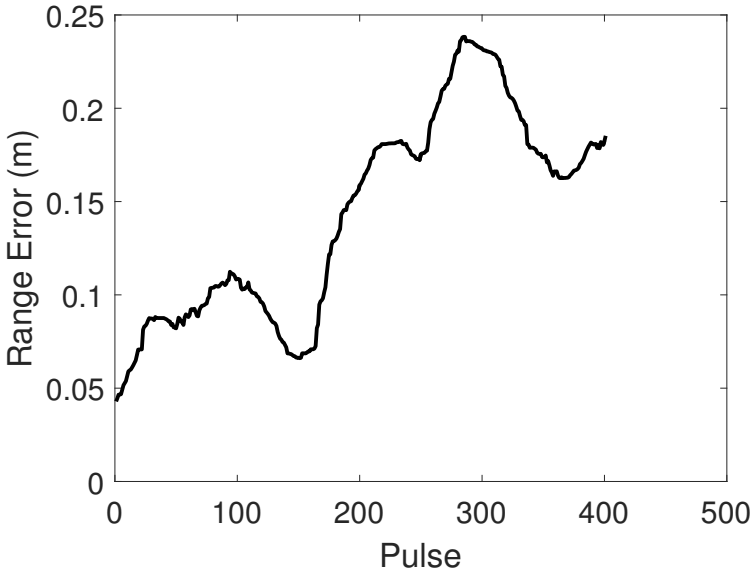

Figure 9. The range error added to each pulse for a scenario with a small residual motion error. Note that the number of pulses is larger than the image shown in Figure 1 as the image was made larger than the scene of interest.

Adding in a large amount of residual motion errors results in many more false detections in the tomographic profile. The resultant range error added to each pulse is shown in Figure 11 and final heights determined are shown in Figure 12. From Figures 11 and 12 it is clear that only a small amount of motion error can be present to gain a reasonable tomographic output, thus constraining the IMU accuracy.

6.5 Understory

If vegetation is present under the canopy (an understory) this may prevent ground returns, especially at X-band. In the simulation the understory is modelled as a homogeneous block volume. If the understory reflectivity is large then the tomographic algorithm mainly detects the top of the understory. This is the case illustrated in Figure 13 where a highly reflective understory is added at 2m. In this case no ground returns are observed as the understory blocks these signals.

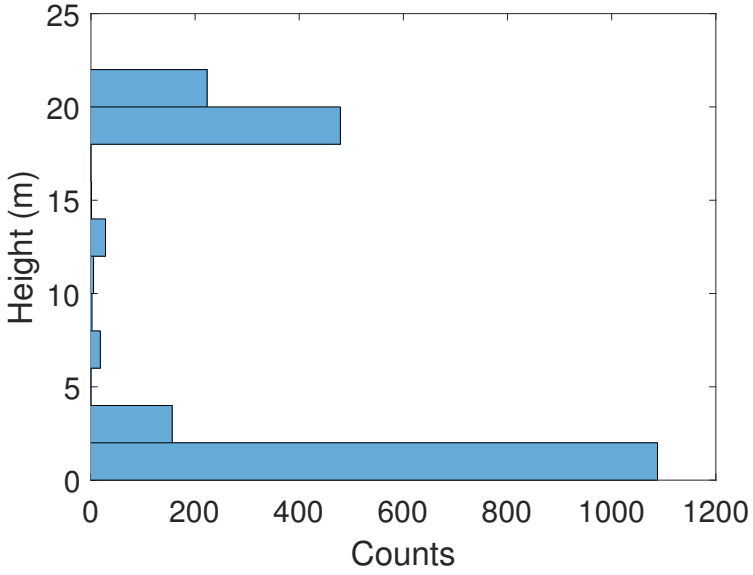

Figure 10. The histogram of heights retrieved from the simple forest scenario with a small residual motion error.

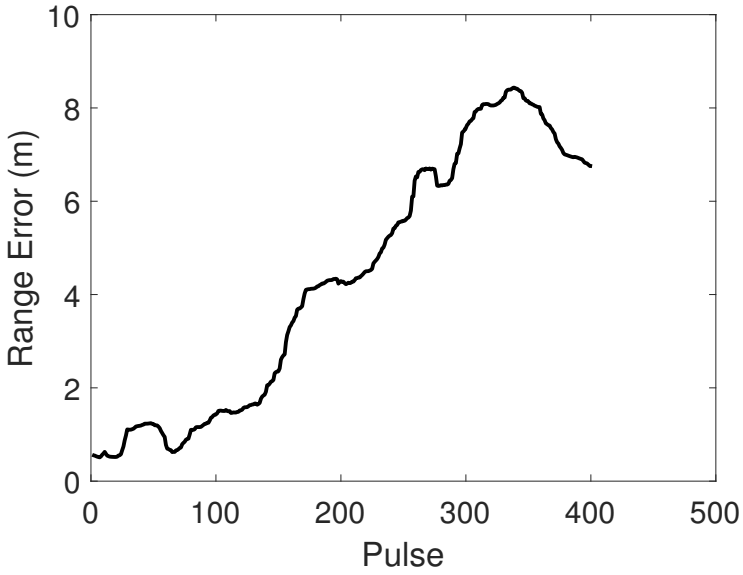

Figure 11. The range error added to each pulse for a scenario with a large residual motion error. Note that the number of pulses is larger than the image shown in Figure 1 as the image was made larger than the scene of interest.

7. DISCUSSION AND CONCLUSION

By simulating helicopter data we analysed the outcome of compressive sensing tomography from a less stable platform. Overall the helicopter motion plays the largest factor in finding an accurate height profile from tomography. The motion error is also related to the flight paths flown. The pilot is unable to fly the helicopter in a straight line path to required tolerances and thus baselines may not be as needed. Decorrelation has a large factor on the outcome from tomography, regardless of the motion error. It should be noted that on a windy day where more decorrelation of the vegetation will occur then the motion errors of the helicopter are likely to be worse. Furthermore forest reflectivities are weather dependent. Having finer SAR image resolution allows for

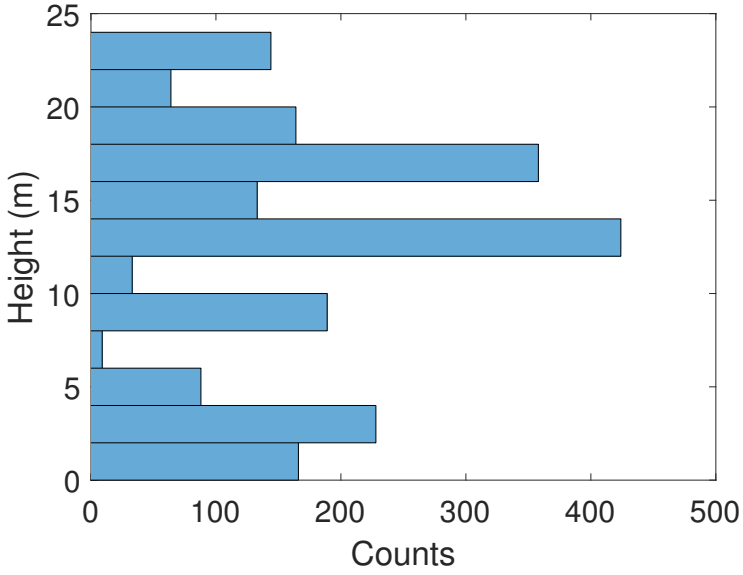

Figure 12. The histogram of heights retrieved from the simple forest scenario with a large residual motion error.

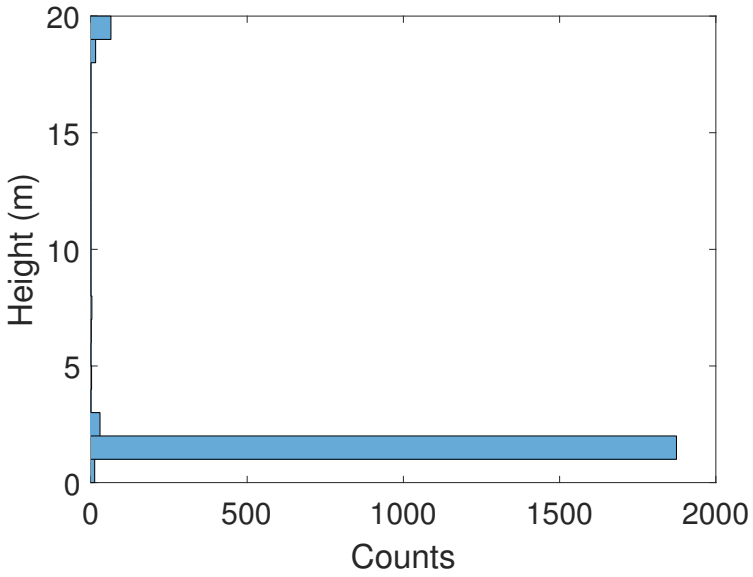

Figure 13. A histogram of the heights retrieved from a forest with a large understory reflectivity. No motion error or decorrelation is added in this scenario.

extra ground signals to be detected in pixels that lie between the canopy. The ground is unlikely to be recovered if an understory is present.

We find that the greedy algorithm is more effective at detecting two or more scatterers in a single pixel. The IHT algorithm occasionally detects sidelobes of the brightest scatterer. For future studies the greedy algorithm would be recommended for tomography purposes.

8. ACKNOWLEDGEMENT

The authors would like to thank Leonardo Ltd for supporting this research.

REFERENCES

[1] Muirhead, F., Halcrow, G., Woodhouse, I. H., Mulgrew, B., and Greig, D., "Compact, low cost, airborne sar interferometry for environmental monitoring," in [*Geoscience and Remote Sensing Symposium (IGARSS), 2015 IEEE International*], 802–805 (July 2015).

[2] Woodhouse, I. H., Izzawati, Wallington, E. D., and Turner, D., "Edge effects on tree height retrieval using x-band interferometry," *IEEE Geoscience and Remote Sensing Letters* **3**, 344–348 (July 2006).

[3] Picard, G., Le Toan, T., and Quegan, S., "A three-dimensional radiative transfer model to interpret ranging scatterometer measurements from a pine forest," *Waves in random media* **14**(2), S317–S332 (2004).

[4] Sun, G. and Ranson, K. J., "A three-dimensional radar backscatter model of forest canopies," *IEEE Transactions on Geoscience and Remote Sensing* **33**, 372–382 (Mar 1995).

[5] Brolly, M. and Woodhouse, I. H., "Vertical backscatter profile of forests predicted by a macroecological plant model," *International journal of remote sensing* **34**(4), 1026–1040 (2013).

[6] Aste, T., "Circle, sphere, and drop packings," *Physical Review E* **53**(3), 2571 (1996).

[7] Cloude, S. R. and Papathanassiou, K. P., "Polarimetric sar interferometry," *IEEE Transactions on Geoscience and Remote Sensing* **36**, 1551–1565 (Sep 1998).

[8] Ulaby, F. T. and Dobson, M. C., "Handbook of radar scattering statistics for terrain.," *ARTECH HOUSE, 685 CANTON STREET, NORWOOD, MA 02062(USA), 1989, 500* (1989).

[9] Richards, J., Woodgate, P., and Skidmore, A., "An explanation of enhanced radar backscattering from flooded forests," *International Journal of Remote Sensing* **8**(7), 1093–1100 (1987).

[10] Siddique, M. A., Hajnsek, I., Aersospace, G., Wegmller, U., and Frey, O., "Investigating the combined use of differential sar tomography and psi for spatio-temporal inversion," in [*Urban Remote Sensing Event (JURSE), 2015 Joint*], 1–4 (March 2015).

[11] Muirhead, F., Mulgrew, B., Woodhouse, I. H., and Greig, D., "Sparsity-driven autofocus for multipass sar tomography," (2015).

[12] S. Chen, C. F. N. C. and Grant, P. M., "Orthogonal Least Squares Learning Algorithm for Radial Basis Function Networks," *IEEE Transactions on Neural Networks* **2**, 302–309 (Mar. 1991).

[13] Mulgrew, B. and Davies, M. E., "Approximate lower bounds for rate-distortion in compressive sensing systems," in [*2008 IEEE International Conference on Acoustics, Speech and Signal Processing*], 3849–3852 (March 2008).

[14] Blumensath, T. and Davies, M. E., "Iterative Thresholding for Sparse Approximations," *The Journal of Fourier Analysis and Applications* , 1–28 (2004).

[15] Jakowatz, C. V., Wahl, D. E., Eichel, P. H., Ghiglia, D. C., and Thompson, P. A., [*Spotlight-Mode Synthetic Aperture Radar: A Signal Processing Approach*], Norwell, MA: Kluwer Academic Publishers (1996).

[16] Kennedy, S., *SAR and Slow-Moving Target Detection*, PhD thesis (2014).